European Journal of Ophthalmology / Vol. 17 no. 3, 2007 / pp. 281-286

Surgical anatomy of the deep lateral orbital wall

U. BEDEN[1], M. EDIZER[2], M. ELMALI[3], N. ICTEN[2], I. GUNGOR[1], Y. SULLU[1], D. ERKAN[1]

[1]Ophthalmology Department
[2]Anatomy Department
[3]Radiology Department, Ondokuz Mayis University, Samsun - Turkey

PURPOSE. *To determine the exact anatomic location and volume of the thickest section of the greater wing of the sphenoid bone (trigone), which is removed during deep lateral orbital wall decompression.*
METHODS. *Eighteen dried skulls were used to determine the exact anatomic location and computed tomography (CT) images of 20 patients (10 male, 10 female) were used for volumetric calculations.*
RESULTS. *Mean values were 14.5 mm for the orbital rim to inferior orbital fissure distance, 23.3 mm for rim to trigone distance, 13.0 mm for width of the trigone base, 5.8 mm for trigone to orbital apex distance, and 12.3 mm for trigone height. The width of the narrowest section of the trigone was 5.2 mm. The trigone was found to have a lower segment (0.92 cc) neighboring the inferior orbital fissure, and an upper segment (0.32 cc) adjoining the thick substance of frontal bone. The narrowest part between these two segments was located just at the superior border of the lateral rectus muscle.*
CONCLUSIONS. *The authors recommend avoiding the thin rectangular portion located in the interfissural area adjacent to the superior orbital fissure. A high intersubject variability underscores the need for individualized preoperative analysis by imaging studies (Eur J Ophthalmol 2007; 17: 281-6)*

KEY WORDS. *Deep lateral orbital wall, Imaging, Surgical anatomy*

Accepted: November 20, 2006

INTRODUCTION

Orbital decompression surgery for Graves' ophthalmopathy has been in existence for almost a century, since first proposed by Dollinger in 1911. The surgery continues to evolve (1-3). Various osteotomy procedures have been utilized for functional and cosmetic reasons in patients with Graves' ophthalmopathy (1-3).
Serious handicaps can result from inferior and medial wall decompression, the most important of which are new onset diplopia and limitations imposed by coexisting pathology in the paranasal sinuses (4-6). These complications have warranted a search for safer techniques, especially when surgery is planned for cosmetic reasons and in patients for whom medial wall resection may not be warranted. The deep lateral orbital wall, in this respect, has been proposed as a potentially safe and effective site for orbital decompression surgery, since it provides much more effective decompression, being a site that is located directly posterior to the globe (7-8). Such surgery has been shown to reduce the risk of postoperative new-onset diplopia relative to medial and, especially, inferior wall decompression (5-7). Orbital surgeons have reported comparable amounts of decompression achieved resecting the lateral wall alone. However, a high degree of anatomic variation between patients has been mentioned (4, 8). Anatomic variations in vital relationships, with structures like the middle cranial fossa, render decompression of the deep lateral orbital wall more difficult, especially for surgeons lacking extensive experience with this procedure, who

 1120-6721/281-06$15.00/0

may have concerns regarding the possibility of dural exposure and cerebrospinal fluid leak (2, 6, 9). In this study, we wanted to assess the exact anatomic localization and volume of the thick segment of the greater wing of the sphenoid bone, the so-called door jamb, which is removed in deep lateral orbital wall decompression.

MATERIALS AND METHODS

Dry skull measurements

Eighteen dried skulls were used to measure the dimensions and determine the location of the thickest section of the greater wing of the sphenoid. A flexible light source was introduced into skulls through the foramen magnum to transilluminate the greater wing of the sphenoid posteriorly, so as to determine the medial and superior border of the thickest section. Another light source was introduced through the temporal fossa to determine the posterior border of the thin section of the lateral wall, where the anterolateral border of the trigone is formed, an area that is not visualized by intracranial transillumination (Fig. 1). After the borders of the trigone were marked, various measurements were taken using a thin flexible ruler (Fig. 1). The skulls then were fixed vertically and pictures of the lateral wall were taken from the 45° medial position over the bridge of the nose at a distance of 10 cm. Surface area calculations of the trigone's reflection to the orbital surface of the greater wing of the sphenoid bone were performed using these pictures. The macro mode of a Canon IXUS 700, 7.2 mega pixel camera was used for photography. A 0.5 × 0.5 cm template fixed atop a thin pointer was introduced into the orbits during photography, to be used as a reference surface area in computerized surface calculations. The pictures then were uploaded onto a personal computer and specific software (Image-pro plus Version 4.5.0.29 for Windows 98/NT/2000, Media Cybernetics Inc.) was used to calculate the surface areas of the orbital reflections of the thick and thin segments of the trigone.

Volume calculations

The volume of the trigone was measured by means of reviewing computerized tomography (CT) images of 20 normal patients (10 male and 10 female), with no orbital disease, who had undergone brain CT angiography imaging procedures (multislice CT [MSCT] 16 detectors, Aquilion 16 systems, Toshiba Medical Systems Corporation, Japan), during which slices of the orbital regions were recorded in 0.5 mm sections to reconstruct highly detailed images. Volumetric calculations of the trigone were performed over the orbital images of these patients. A lower and upper point was set to measure the volume of the trigone. The lower point was defined as the point at which the trigone begins inferiorly, lateral to the tip of the inferior orbital fissure; the upper point was defined as the junction of the lateral wall and the roof of the orbits. The volume and height of the trigone were measured in two stages, pertaining to two segments of the trigone. The first stage involved starting from the base of the trigone and extending to the superior border of the lateral rectus muscle, where the trigone was found to be least thick before it starts to thicken again; from there, the segment extends from the point just described to the thick part of the frontal bone (Fig. 2). The volume and height of the second segment was measured starting from the superior border of the lateral rectus, extending superolaterally to the junction of the roof and the lateral wall of the orbit. The heights and volumes of the two segments were noted separately. The measured heights were not true heights of the thick part of the lateral wing, because the anterosuperior and posteroinferior portions are not aligned sagittally. However, heights were measured according to the number of slices used after the upper and lower limits were determined, indicating the vertical reflection of all thick segments of the lateral wall.

Statistical analysis

All volume and surface parameters were measured to three decimal places. All other parameters were recorded with no decimals. Descriptive statistics (mean, minimum, maximum, standard deviation, et cetera) were evaluated for all parameters collected from dry skull measurements. Since all the measurements, including the volume calculations, exhibited a normal distribution, Student *t*-tests were used to examine for intersex differences. To determine the relationships between various characteristics, Pearson correlation coefficients (r) and determination coefficients (r^2) were calculated to estimate the strength of

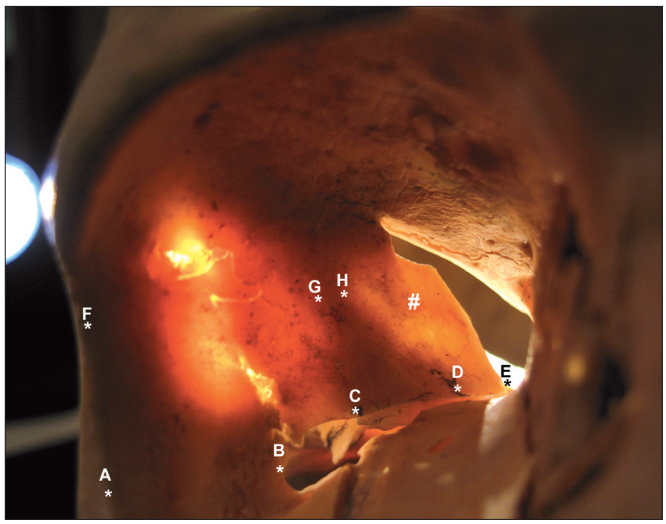

Fig. 1 - *Measurements at various distances for exact location of the thick substance of the greater wing of the sphenoid. A-B: Rim-inferior orbital fissure distance; A-C: rim-trigone distance; C-D: width of the base of the trigone; D-E: trigone-orbital apex distance; F-G: rim-trigone distance at narrowest part of trigone; G-H: width of the narrowest part of the trigone; G-C: height of the trigone (distance between base and narrowest part of trigone); #: the thin part of the greater wing, neighboring the superior orbital fissure and middle cranial fossa.*

Fig. 2 - *Image showing the narrowest part of the trigone at the upper border of the lateral rectus muscle (arrow). 3D bone density image; *lateral rectus muscle.*

the correlations and the degree of variance in one measure determined by the other, respectively. Regression analysis also was conducted to assess whether there is any significant effect of age on the volume of the thick part of the lateral wall. For all analyses, $p<0.05$ was accepted as statistically significant, while $p<0.01$ was accepted as highly significant. Statistical aid was supplied by the Department of Biostatistics, Medical Faculty, Ondokuz Mayıs University. Analyses were performed using SPSS, release 13.01, Statistical Package Program.

RESULTS

Measurements from 18 dried skulls and CT images of 20 subjects (10 male and 10 female, mean age 49.20±11.60 years) were completed.

Transillumination revealed that the first thick part of the greater wing of the sphenoid is located posteroinferiorly (on the inferomedial surface of the lateral wall), adjacent to the inferior orbital fissure. This thick segment blends with the second thick segment, which is located anterosuperiorly (in the superolateral section

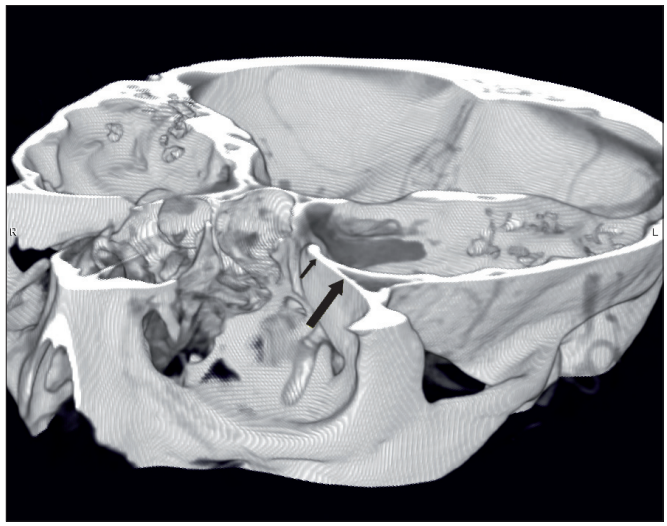

Fig. 3 - *Three-dimensional bone density image, demonstrating the thick (larger arrow) and thin segments (small arrow) of the lateral orbital wall adjacent to middle cranial fossa between the superior and inferior orbital fissures.*

of the lateral wall) through a narrow band before it blends to the thick substance of frontal bone. Hence, the horizontally narrowest segment of the thick mass of the lateral orbital wall is located at the junction of

the posteriorly located inferomedial and anteriorly located superolateral thick segments of the sphenoid's greater wing. Thus, medial to the narrowest part is the thin part of the greater wing located just inferolateral to the superior orbital fissure, which is immediately adjacent to the middle cranial fossa. This part also was determined, during volumetric studies, to be at the level of the superior border of the lateral rectus muscle. The measured parameters are given in Table I.

Pearson correlation analysis revealed positive and negative correlations among the parameters obtained from the dry skull measurements. Significant results are given in Table II.

Volume calculations and descriptives are presented in Table III.

No significant differences were detected between males

TABLE I - PARAMETERS RECORDED BY MEASUREMENT OF DRIED SKULLS

	Mean (mm)	Standard deviation	Minimum (mm)	Maximum (mm)
R-IOF	14.5	1.870	12	17
R-T	23.3	3.076	20	29
WTB	13.0	2.280	9	15
T-OA	5.8	1.602	4	8
R-TN	20.5	3.391	16	24
TH	12,3	2,503	10	16
WTN	5.2	4.997	2	12
STK, cm^2	1.871	0.996	0.658	3.150
STN, cm^2	0.898	0.563	0.427	1.865

R-IOF = Rim-inferior orbital fissure distance; R-T = Rim-trigone distance; WTB = Width of trigone base; T-OA = Trigone-orbital apex distance; R-TN = Rim-trigone's thinnest part distance; TH = Height of trigone; WTN = Width of the thinnest part of the trigone; STK = Surface of the thick segment of the greater wing; STN = Surface of the thin segment of the greater wing

TABLE II - SIGNIFICANT CORRELATIONS DETECTED AMONG THE DIMENSIONS MEASURED FROM DRIED SKULLS

Parameters	Correlation coefficient (r)	Determination coefficient (r^2)	p value
R-IOF, R-TN	0.731	0.535	0.016
R-IOF, WTN	–0.436	0.190	0.033
R-IOF, STK	–0.502	0.252	0.034
WTB, WTN	–0.493	0.243	0.007
R-TN, WTN	–0.998	0.996	<0.001
WTN, STK	0.840	0.706	<0.001
WTN, STN	–0.772	0.596	<0.001
STK, STN	–0.858	0.736	<0.001

R-IOF = Rim-inferior orbital fissure distance; R-TN = Rim-trigone's thinnest part distance; WTN = Width of the thinnest part of the trigone; STK = Surface of the thick segment of the greater wing; WTB = Width of trigone base; STN = Surface of the thin segment of the greater wing

TABLE III - RESULTS OF VOLUME AND HEIGHT MEASUREMENTS PERFORMED ON CT IMAGES

	Mean	Standard deviation	Minimum	Maximum
Volume of lower segment (cc)	0.92	0.37	0.43	1.66
Height of lower segment (mm)	15.45	2.63	12.00	20.00
Volume of upper segment (cc)	0.32	0.17	0.11	0.77
Height of upper segment (mm)	4.60	1.47	3.00	7.00
Total volume (cc)	1.24	0.45	0.54	2.39
Total height (mm)	20.05	2.72	15	25
Age of patients (yr)	49.20	11.60	36	80

and females, except for the height of the trigone (male/female: 15.8 mm/15.1 mm, p=0.036). Regression analysis revealed no correlation between the various parameters and subject age, as expected, since all measurements were taken from adult subjects.

DISCUSSION

The high incidence of diplopia (as high as 63%) after orbital decompression surgery has prompted a search for safer surgical techniques over the past few decades, especially since the operation is undertaken not only for functional reasons, but also for the esthetic rehabilitation of patients with Graves' ophthalmopathy (2, 3, 10). Largely in response to a report by Goldberg et al (8), the lateral orbital wall has gained increasing popularity as a relatively safe site for decompression surgery. In the lateral orbital wall, the thin section starts to thicken about 1 cm posterior to the zygomaticosphenoid suture, where it divides to form the anterior corner of the middle cranial fossa (11). Here, the bone thickens to form a trigone, which Goldberg et al have called the door jamb, stressing the importance of this zone as a convenient place for orbital decompression surgery, allowing a considerable amount of lateral and posterior expansion of the orbit to be achieved (8, 12). Goldberg et al (12) reported an average of 5.9 mm of reduction in exophthalmos with extensive lateral wall resection only, which offers 0 to 0.5 mm reduction in proptosis for each mm^3 of orbital volume expansion, due to its location exactly posterior to the globe. It has been reported that removal of the lateral wall up to 25 mm from the orbital rim yields only 2 to 2.9 cc of volume (0.54 to 2.39 cc in our study) (8, 13, 14). However, the decompression effect has been proposed to be greater in practice, because opening the temporalis fascia and removing muscle tends to yield much more available space (14).

The lateral wall is supposed to have the lowest complication rate, when used for decompression (15). Ben Simon et al (5) reported that they were able to convert to a deep lateral wall decompression with fat debulking as a first-line surgical treatment, to reduce the risk of postoperative strabismus, which is higher in patients with preoperative muscle restriction and diplopia. However, some other potential complications that have been reported are stroke, death, visual loss, cerebrospinal fluid leak, paresthesia in lacrimal and zygomatic regions, lateral canthal misalignment, and intraorbital hemorrhage (2, 5).

In deep lateral wall decompression, the frontal segment of the lacrimal fossa is thinned to provide additional space for lacrimal gland herniation. Bone removal then is continued posteroinferiorly, including the trigone of the greater wing of the sphenoid, which lies anterior to the temporal lobe of the brain (9). Bleeding and dural exposure leading to cerebrospinal fluid leak can be encountered during this stage, but the risk can be minimized with extreme care (9).

The contribution of deep lateral wall resection to exophthalmos reduction also has been assessed in prior studies, as has its potential influence on the onset of consecutive diplopia (4). Baldeschie et al (4) stated that removal of the deep lateral wall contributes to exophthalmos reduction by 2.3 mm, with a 13% incidence of new-onset diplopia, which resolves spontaneously in 4 to 6 months. However, the authors reported a twofold greater standard deviation in exophthalmos reduction with deep lateral wall removal versus classical three-wall decompression surgery, which stresses the importance of variability between patients (4). The results of our study confirmed this intersubject variability, which also has been reported by Goldberg et al (8). This high intersubject variability and the risk of serious complications, like cerebrospinal fluid leak, might be responsible for this technique not having gained as much popularity as other techniques, like balanced decompression. It also has been reported by experienced surgeons that anatomic familiarity is an important requisite for the procedure (6, 12).

Negative correlations were detected in our study between orbital rim-trigone's thinnest part distance and thickness of the thinnest part of the trigone. Negative correlations also were evident between the surface area of the thick and thin sections of the greater wing. This could have been predicted, since the sum of two gives a constant amount in the former and latter instances. However, other correlations like the positive correlations between thickness of the narrowest part and surface area of the trigone, and the negative correlation between the orbital rim-inferior fissure distance and thickness of the narrowest part of the trigone, and between distance from the orbital rim to the inferior fissure and trigone surface area, are quite useful relationships that might be used during surgery. Keeping in mind the minimum and maximum values of various parameters, one can predict other values during surgery, so that some of the complications reported above can be avoided.

The thick section of the greater wing has been described

as the narrow space between the inferior and superior orbital fissures (2, 5). However, the thin part of the lateral wall adjacent to the superior orbital fissure should be kept in mind during the procedure. The findings of our study suggest that removal of deep lateral wall should be started inferiorly, just lateral to the inferior orbital fissure and then extended superolaterally, just as reported by Baldechi et al (4). Care should be taken during this step to preserve the quadrangular thin part of the greater wing that lies below the superior orbital fissure, which in turn is adjacent to the middle cranial fossa, in order to avoid exposure of the dura matter (Figs. 1 and 3). The high degree of intersubject variability in the various parameters, as reported previously and found in our study, renders imaging studies necessary in the planning stage of the operation for each patient, in order to have a preoperative assessment regarding the thin and thick segments of the deep lateral wall.

In this study, we provided average dimensions and locations of the thick segment of the greater wing of the sphenoid, all of which can be used as anatomic guidelines during deep lateral orbital decompression surgery. The variability encountered in this study underscores the need for individualized preoperative analysis by imaging studies.

None of the authors has any financial interest in products mentioned in this article.

Reprint requests to:
Umit Beden, MD
Ondokuz Mayıs University
Ophthalmology Department
55139, Kurupelit
Samsun, Turkey
umite@yahoo.com

REFERENCES

1. Frankel J. Old wine and new wine. Arch Ophthalmol 2000; 118: 1006-7.
2. Graham SM, Brown CL, Carter KD, Song A, Nerad JA. Medial and lateral orbital wall surgery for balanced decompression in thyroid eye disease. Laryngoscope 2003; 113: 1206-9.
3. Bonavolontà G. Evolution of the lateral orbitotomy (coronal approach to the orbit). Acta XXIV International Congress of Ophthalmology. San Francisco: 1982; 2: 1036-9.
4. Baldeschi L, MacAndie K, Hintschich C, Wakelkamp IMMJ, Prummel MF, Wiersinga WM. The removal of the deep lateral wall in orbital decompression: its contribution to exophthalmos reduction and influence on consecutive diplopia. Am J Ophthalmol 2005; 140: 642-7.
5. Ben Simon GJ, Wang L, McCann JD, Goldberg RA. Primary-gaze diplopia in patients with thyroid-related orbitopathy undergoing deep lateral orbital decompression with intraconal fat debulking: a retrospective analysis of treatment outcome. Thyroid 2004; 14: 379-83.
6. Goldberg RA, Perry JD, Hortaleza V, Tong JT. Strabismus after balanced medial plus lateral wall versus lateral wall only orbital decompression for dysthyroid orbitopathy. Ophthal Plast Reconstr Surg 2000; 16: 271-7.
7. Goldberg RA. The evolving paradigm of orbital decompression surgery. Arch Ophthalmol 1998; 116: 95-6.
8. Goldberg RA, Kim AJ, Kerivan KM. The lacrimal keyhole, orbital door jamb, and basin of the inferior orbital fissure. Arch Ophthalmol 1998; 116: 1618-24.
9. Ünal M, İleri F, Konuk O, Hasanreisoglu B. Balanced orbital decompression combined with fat removal in graves ophthalmopathy. Ophthal Plast Reconstr Surg 2003; 19: 112-8.
10. McCord CD. Current trends in orbital decompression. Ophthalmology 1985; 92: 21-33.
11. Dutton JJ. Osteology of the orbit. In: Dutton JJ, ed. Clinical and Surgical Anatomy of the Orbit. Philadelphia: WB Sounders Company; 1994: 1-12.
12. Goldberg RA, Weinberg DA, Shorr N, Wirta D. Maximal, three-wall, orbital decompression through a coronal approach. Ophthalmic Surg Lasers 1997; 28: 832-43.
13. Pearl RM, Vistnes L, Troxel S. Treatment of exophthalmos. Plast Reconstr Surg 1991; 87: 236-44.
14. Stabile JR, Trokel MS. Increase in orbital volume obtained by decompression in dried skulls. Am J Ophthalmol 1983; 95: 327-31.
15. Kazım M. Commentary on “Orbital decompression.” Ophthal Plast Reconstr Surg 2003; 19: 445.